10.21611/qirt.2022.2001

QIRT'2022 16th Quantitative InfraRed Thermography Conference

Automated object recognition of circular defects using infrared thermographic

by Seungju Lee*, Yoonjae Chung** and Wontae Kim***, †

* Department of Future Convergence Engineering, Kongju National University, 1223-24 Cheonan-Daero, Seobuk-gu, Cheonan-si 31080, Korea; cow123456798@smail.kongju.ac.kr
** Eco-Sustainable Energy Research Institute, Kongju Natioanl University, 1223-24 Cheonan-Daero, Seobuk-gu, Cheonan-si 31080, Korea ; dbswosla79@kongju.ac.kr
*** † D□□□ of Mechanical & Automotive Engineering, Kongju National University, 1223-24 Cheonan-Daero, Seobuk-gu1, Cheonan-si 31080, Korea; kwt@kongju.ac.kr

Abstract

Active infrared thermography is an attractive and reliable technique due to its non-contact, large-area, high-speed, qualitative and quantitative characteristics. In the lock-in infrared thermography, a lot of noise was generated due to non-uniform heat source excitation, so filtering was applied. The optimal excitation frequency for each amplitude and phase was calculated using the ROI technique, and the automatic defect detection of circular defects was performed by applying the binarization processing algorithm. In this study, a mechanism that can perform clear defect detection in a very fast time was presented.

1. Introduction

Aluminum is a metal with high thermal conductivity and good corrosion resistance. Although it has low strength, it has excellent weldability and workability, so it is used in various fields such as machinery, aerospace, chemical plants, sports, automobiles and ships. However, defects often occur during production, processing and maintenance, and non-destructive evaluation techniques for stable operation are very important.

In order to secure the performance and safety of various machines and structures, non-destructive testing is being carried out in each field of industry. If there is no defect in the material or product, it is designed and used according to the data obtained by the mechanical strength test of the defect-free material. However, in reality, it is difficult to expect perfect materials, and new defects occur during used and operation. In recent years, the risk of corrosion, radiation, flammability and explosiveness is increasing according to the environment of materials use, so securing safety for condition monitoring and accident prevention is becoming more important.

Currently, non-destructive inspection techniques that are widely used include visual inspection(VT) for surface defects, penetrant inspection(PT), magnetic particle inspection(MT), eddy current inspection(ECT) and infrared thermography(IRT). Radiographic inspection(RT) and ultrasonic inspection(UT) are mainly used for internal defect inspection[1]. In addition to these inspection methods, various non-destructive inspections are being applied, but there is a limit to detecting all existing defects, and research and development of many new technologies are in progress to overcome these limitations. IRT, which is one of the non-destructive inspection techniques, is non-contact based, measures the radiant energy of the object surface with an IR camera, converts the electrical signal into a thermal signal as a 2D image, and displays a thermal image in real time[2,3]. It has non-penetrating and non-contact characteristics with respect to an object, and it is possible to observe a wide area. In addition, real-time temperature analysis is possible, so it is being used for various purposes throughout the industry.

In this paper, automated detection of defects on the back surface of aluminium plates was performed using lock-in thermography(LIT), one of the IRT techniques. Phase and amplitude images were acquired using a 4-point signal processing, and the optimal frequency was derived. Then, after improving the detectability by applying 1st and 2nd de-noising, automatic defect detection was performed using the boundary tracking algorithm.

2. Theoretical background

2.1. 4-point signal process

LIT is a technique for acquiring changes in phase and amplitude by processing a response signal generated after a high-frequency function-type heat source is incident on an object to be inspected[4]. When heat source energy reaches the surface of an object, it is absorbed and the phase shifts. When energy reaches a region within an object with non-uniform thermophysical properties, the incident energy is partially reflected. The reflected energy interferes with the energy incident on the surface of the object, causing an interference pattern of local surface temperature that vibrates at the same frequency as the heat wave[5]. For a flat plate, the temperature field with heat wave is as follows:

$$\frac{\partial T}{\partial t} = \frac{k}{\rho c_p}\frac{\partial^2 T}{\partial x^2} \quad (1)$$

Where T is temperature, t is time, k is thermal conductivity, ρ is density, c_p is specific heat and x is the distance in the heat flow direction. The heat wave heated in the form of a harmonic function is as follows:

$$\mathrm{T(x.t)} = T_0 e^{-x/\mu}\cos\left(wt - \frac{x}{\mu}\right) \quad (2)$$

$$\mu = \sqrt{\frac{2\alpha}{w}} = \sqrt{\frac{\alpha}{\pi f}} \quad (3)$$

$$\alpha = \frac{k}{\rho c_p} \quad (4)$$

Where T_0 is the initial temperature generated by the heat source, ω is the modulation frequency, μ is the penetration depth, α is the thermal diffusion coefficient and f is the frequency.

In the LIT technique, an external sine wave heat source is incident on the plate, and the response temperature signal records a 2D thermal distribution image in real time using an infrared system. A 4-point signal process is used to convert the phase and amplitude data of a 2D image generated by a heat source in the form of a sine wave. Figure 1 shows the principle of the 4-point method. When there are four constant distance temperature data S1, S2, S3 and S4, the phase and amplitude are as follows:

$$\emptyset = tan^{-1}\left(\frac{S_1 - S_3}{S_2 - S_4}\right) \quad (5)$$

$$\mathrm{A} = \sqrt{(S_1 - S_3)^2 + (S_2 - S_4)^2} \quad (6)$$

The reflected heat wave is determined by its amplitude, phase and modulation frequency. The principle of defect detection is based on the fact that the defective area has a phase delay with respect to the sound area, and high-level quantitative data can be obtained by utilizing the 4-point signal processing.

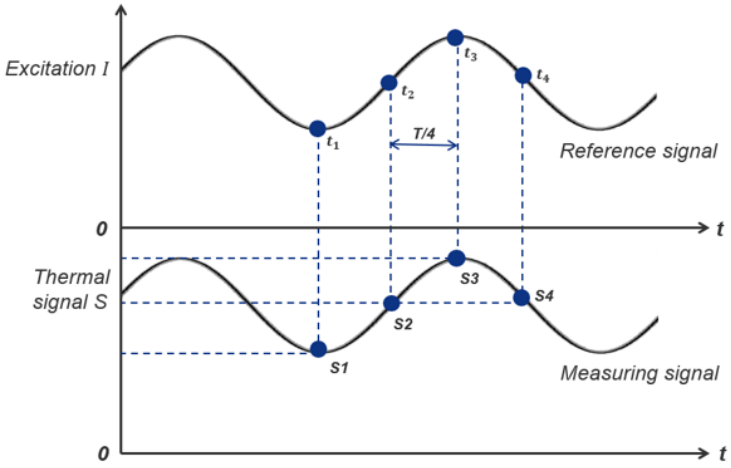

Fig. 1. *4-point signal process principle of LIT*

2.2. Binary process

There are many techniques for image analysis, and the simplest and fastest technique among them is to use a threshold to binarize an image[6,7]. It is used in many pre-processing steps in image processing, such as separating the background from objects in an image, extracting only pixels with a brightness value above a certain level, or simplifying the entire information in an image. The Otsu algorithm is the most representative method for probability calculating the threshold value of an image.

The Otsu algorithm is a method of calculating the optimal threshold that can classify images into two classes by using a histogram based on gray scale. Based on the threshold value k in the binarized image, [0,k] is classified as 'class 1' and [k+1] is 'class 2'. Through this process, a binarized image can be obtained. In general, converting a 2D thermal image into a binarized image can clearly characterize the location of the defect.

In order to classify the two binarized images, it is necessary to calculate an optimal threshold. When there is an M×N size image with L intensity levels like 0, 1, 2, …, L-1, pixels with intensity values in [0,k] are classified as class 1, and intensity values in [k+1, L-1] are classified as class 2. The probability that a pixel is classified into class 1 and class 2 is as follows:

$$P_1(k) = \sum_{i=0}^{k} P_i \tag{7}$$

$$P_2(k) = 1 - P_1(k) \tag{8}$$

The average intensity values of the pixels classified into class 1 and class 2 are as follows:

$$m_1(k) = \frac{1}{P_1(k)} \sum_{i=0}^{k} iP_i \tag{9}$$

The average intensity values up to the k level among all images are as follows:

$$m_G = P_1 m_1 + P_2 m_2 \tag{10}$$

To calculate the optimal threshold, the Otsu algorithm should apply the concept of between-class variance, as follows:

$$\sigma_b^2 = \frac{(m_G P_1 - m)^2}{P_1(1 - P_1)} \tag{11}$$

Calculating the optimal k value is a simple principle, but it can be calculated only by substituting all k values in the intensity range [0, L-1]. The k value was calculated using MATLAB software, and the principle of the Otsu algorithm is to classify the binarization based on the k value obtained in this way.

3. Experiment setup of LIT

3.1. Specimen

In this study, plate specimen made of aluminium was used. There are circular artificial defects of various aspect ratios, the row axis being the same depth length and the column axis being the same diameter. Figure 2 shows the overall dimensions of the specimen, with a thickness of 10 mm and a square plate of 180×180 mm. Additionally, 16 defects present in the plate are marked with unique indexing. The front side of the plate was coated with KRYLON black paint to maintain the emissivity of 0.95 or higher, and Figure 3 shows the shape of the front and back. Table 1 shows the thermal properties of aluminium.

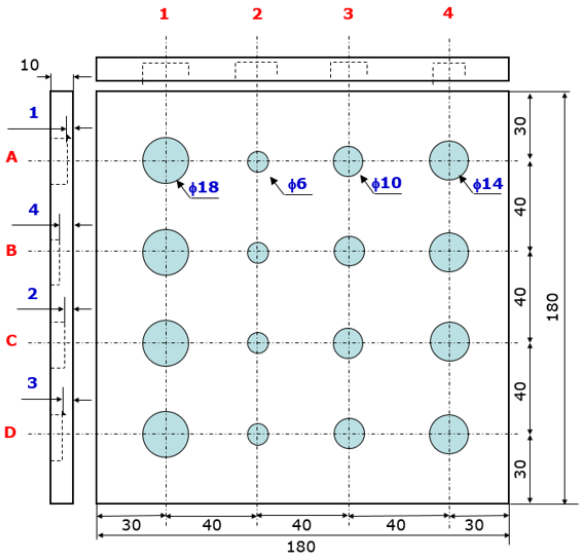

Fig. 2. *Dimension schematic for circular defects in aluminium plate*

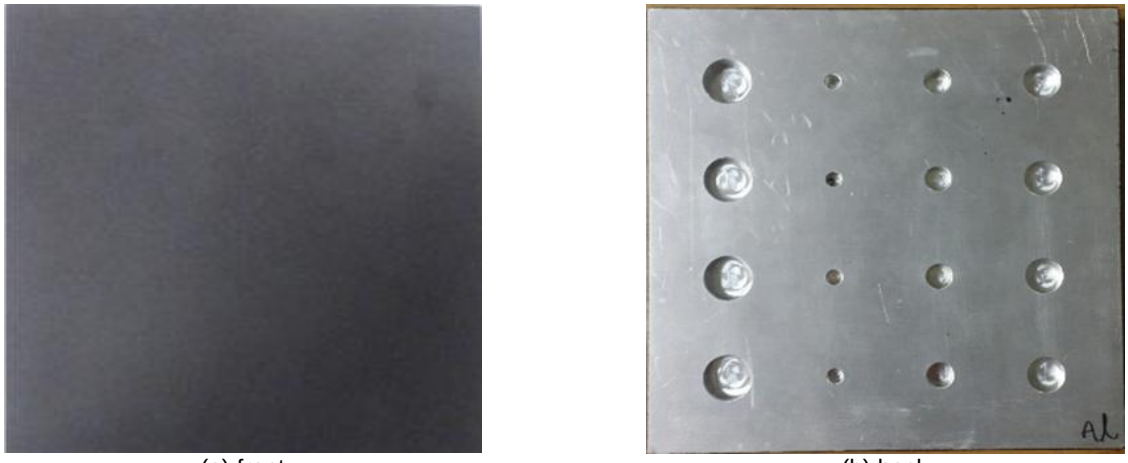

(a) front (b) back

Fig. 3. *Front and back of aluminium specimen*

Table 1. *Thermal properties of aluminium specimen*

Thermal Conductivity	210 $\mathrm{W/m \cdot K}$
Specific Heat	921 $\mathrm{J/kg \cdot K}$
Thermal Diffusivity	$9.7\times 10^{-5}\ m^2/s$
Density	2700 kg/m^3
Initial Temperature	22℃

3.2. Experimental system of LIT

Figure 4 shows the configuration of the experimental devices for the LIT technique used in this study. Heat is provided by two 1 kW halogen lamps as heat sources, controlled by a power amplifier and function generator. The temperature response signal generated by the heat source was measured by an IR camera of the SC645 (un-cooled, 640×480 pixels, 7.5 ~ 13 μm) model. A frame rate of 50 Hz was set for 4-point signal processing. The excitation frequency was adjusted in steps of 0.01 Hz in the range of 0.01 to 0.1 Hz. Thermal images were acquired using commercial FLIR R&D software.

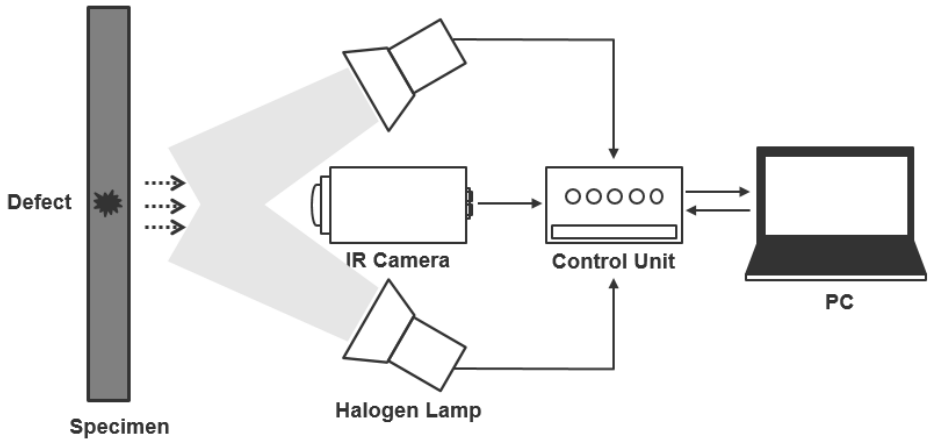

Fig. 4. *Infrared experimental system for defect detection in LIT*

4. Results

4.1. Optimal excitation frequency

Phase and amplitude images were acquired by calculating the 4-point signal process of the LIT technique. Then, the SNR of the ROI was calculated to find the optimal frequency among the excitation frequency ranges. The average value of the 5×5 pixel area was calculated for the defective area and the sound area of the ROI, and the SNR equation is as follows[8,9]:

$$\mathrm{SNR} = 20log_{10}(\frac{|DROI_{mean} - SROI_{mean}|}{\sigma}) \quad (12)$$

Where $DROI_{mean}$ and $SROI_{mean}$ are the arithmetic mean of all the pixels in the defective area and the sound area, respectively, and σ is the standard deviation of all the pixels in the sound area.

Figure 5 shows the SNR values for each excitation frequency of phase and amplitude. The highest SNR value can be seen at 0.01 Hz for phase and 0.02 Hz for amplitude. In addition, it can be seen that the amplitude data is quantitatively excellent because the SNR value of the amplitude is high overall.

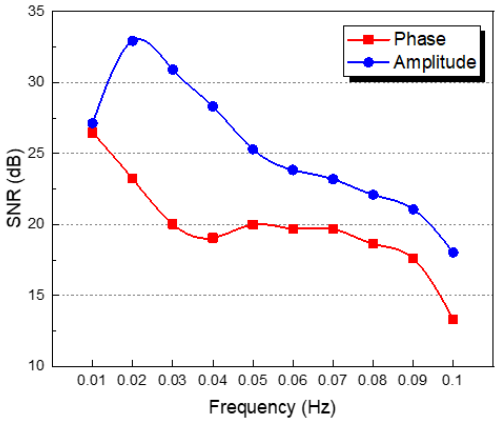

Fig. 5. *SNR graph of phase and amplitude of excitation frequency range*

4.2. Filtering(1st de-noising)

After calculating the optimal excitation frequency for 1st de-noising, filtering was applied to each image. The applied filtering was Median, Gaussian and NLmeans filtering, and the detectability was compared and analysed using the SNR equation. Figure 6 shows the raw image(non-filtering) and the filtered image, and Table 2 shows the SNR value for each image. Both phase and amplitude can confirm the highest detectability improvement in Median Filtering, and Gaussian and NLmeans filtering tend to decrease detectability, which requires a change in the previously used Kernel Mask.

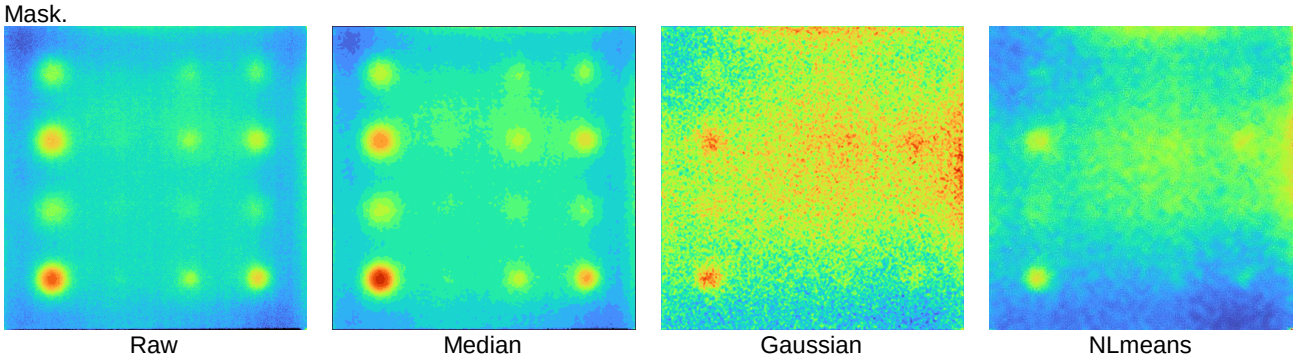

Raw Median Gaussian NLmeans

(a) phase

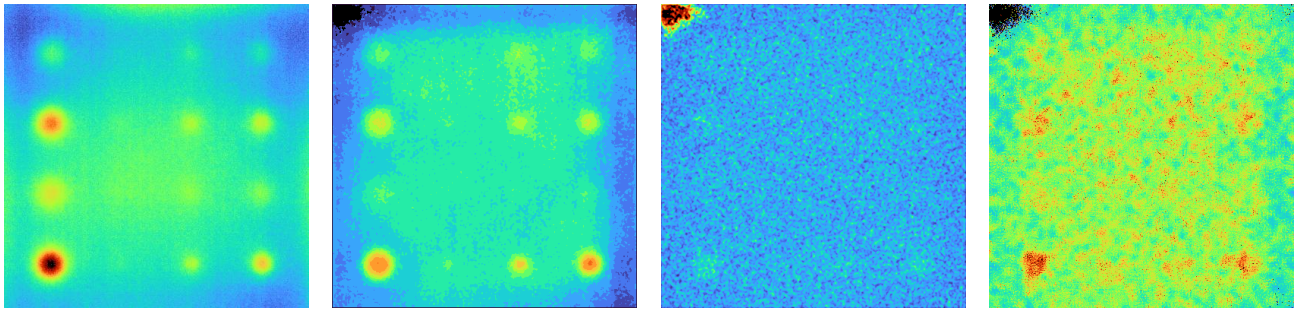

Raw Median Gaussian NLmeans

(b) amplitude

Fig. 6. *2D thermal images of phase and amplitude filtering applied*

Table 2. *SNR values of filtered 2D thermal image*

	Raw	Median	Gaussian	NLmeans
Phase	26.476	27.432	6.722	14.196
Amplitude	32.929	35.705	17.299	22.071

4.3. Morphological operation(2nd de-noising)

The Otsu algorithm was applied to perform binarization processing on the image to which 1st de-noising(Median filtering) was applied. The phase and amplitude thresholds were calculated as 16 and 19, and are classified into class 1 and class 2 based on the threshold values. Figure 7 shows a binarized image, and it can be confirmed that noise is present.

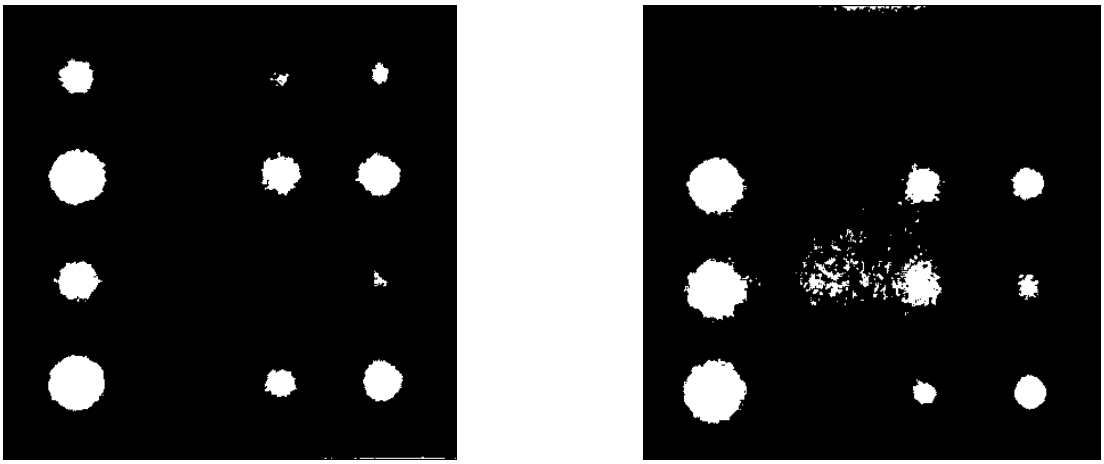

(a) phase (b) amplitude

Fig. 7. *Binarized image of 2D thermal image with the Otsu algorithm applied*

Morphological operation was performed to remove noise. ‘bwareaopen’, ‘strel’ and ‘imfill’ functions were applied, and Figure 8 shows a binarized image with morphological operation applied. In order to apply boundary tracking, an automatic object recognition algorithm, it is necessary that the boundary of the object be smooth.

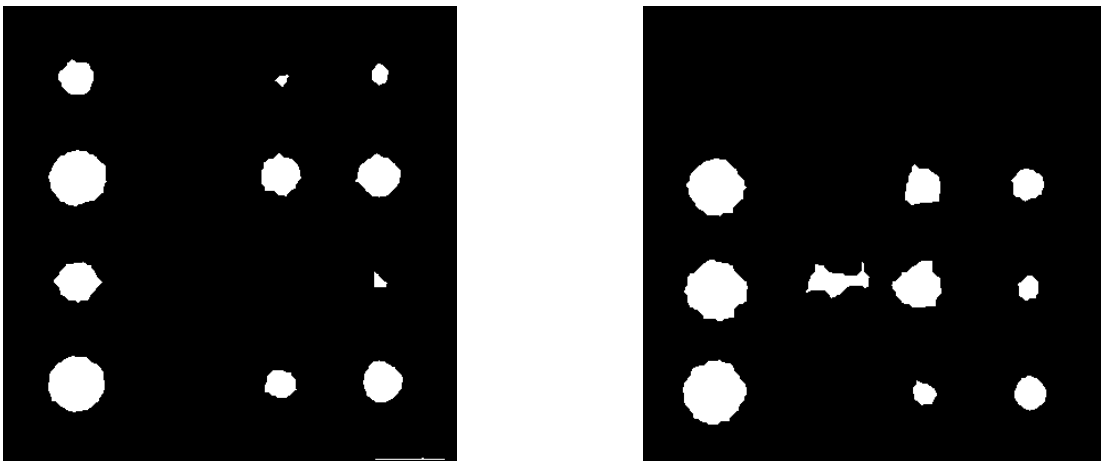

(a) phase (b) amplitude

Fig. 8. *Binarized image with de-noising by applying morphological operation*

4.4. Automatic object recognition

After 1st and 2nd de-noising was applied, an automated algorithm was applied to recognize defective objects in the image. Boundary tracking algorithm uses circularity metric to determine whether a circular object is defective after tracking the boundary of an object. Circularity metric is as follows[10,11]:

$$\text{Metric} = \frac{4\pi \times area}{perimeter^2} \tag{13}$$

This metric means that the closer it is to 1, the closer it is to a circular shape. Also, it can be used only to recognize a circular object. The circular reading standard threshold set in this study was set to 0.7 and Figure 9 shows the image to which the algorithm is applied.

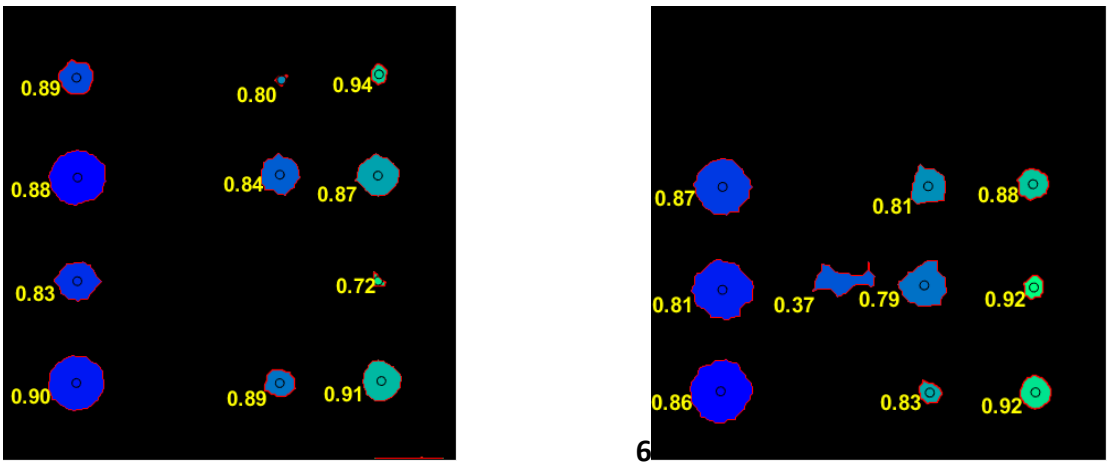

(a) phase (b) amplitude

Fig. 9. *Circular defect detection using automatic object recognition algorithm*

It can be seen that 11 defects were detected in phase and 9 defects were detected in amplitude. Quantitatively, the amplitude data was good, but the qualitative analysis for defect identification was better in the phase. Also, in the amplitude image, both the 1st row and 2nd column defects failed to be detected, which can be regarded as the effect caused by the non-uniform heat source excitation.

Optical IRT has a non-uniform heat source and generates a lot of noise compared to other techniques, so signal processing and filtering must be applied. However, it has the advantage of obtaining quantitatively excellent data, so it can be applied to various materials.

5. Conclusions

In this study, the back-side defect detection in the aluminium plate was performed using the LIT technique. Phase and amplitude data were acquired using 4-point signal processing, filtering was applied to improve the 1st de-noising detectability, and the performance of Median filtering was the best. After that, the Otsu algorithm was applied to acquire the binarized image, and morphological operation was performed for the 2nd de-noising. Finally, automated defect detection was performed using the boundary tracking algorithm. Defects were detected with 11 in phases and 9 in amplitude, and it is difficult to detect defects with a small diameter or shallow depth. This requires uniform heat source excitation, and future research will develop a calibration algorithm mechanism that can overcome the limitations of non-uniform heat source.

REFERENCES

[1] Maldague, X. (2001). Nondestructive Testing Handbook. 3. Infrared and Thermal Testing. American Society for Nondestructive Testing: Arlingate Lane, OA, USA.
[2] Usamentiaga, R., Venegas, P., Guerediaga, J., Vega, L., Molleda, J., & Bulnes, F. G. (2014). Infrared thermography for temperature measurement and non-destructive testing. Sensors, 14(7), 12305-12348.
[3] Shrestha, R., & Kim, W. (2018). Evaluation of coating thickness by thermal wave imaging: A comparative study of pulsed and lock-in infrared thermography–Part II: Experimental investigation. Infrared Physics & Technology, 92, 24-29.
[4] Breitenstein, O., & Langenkamp, M. (2003). Lock-in thermography. In Basics and Use for Functional Diagnostics of Electronics Components. Springer-Verlag Berlin Heidelberg.
[5] Meola, C., Carlomagno, G. M., Squillace, A., & Vitiello, A. (2006). Non-destructive evaluation of aerospace materials with lock-in thermography. Engineering failure analysis, 13(3), 380-388.
[6] Chung, Y., Shrestha, R., Lee, S., & Kim, W. (2022). Binarization Mechanism Evaluation for Water Ingress Detectability in Honeycomb Sandwich Structure Using Lock-In Thermography. Materials, 15(6), 2333.
[7] Zhan, Y., & Zhang, G. (2019). An improved OTSU algorithm using histogram accumulation moment for ore segmentation. Symmetry, 11(3), 431.

[8] Tang, Q., Bu, C., Liu, Y., Qi, L., & Yu, Z. (2015). A new signal processing algorithm of pulsed infrared thermography. Infrared Physics & Technology, 68, 173-178.
[9] Chung, Y., Shrestha, R., Lee, S., & Kim, W. (2020). Thermographic inspection of internal defects in steel structures: analysis of signal processing techniques in pulsed thermography. Sensors, 20(21), 6015.
[10] Lee, S., Chung, Y., Shrestha, R., & Kim, W. (2021). Automated Defect Detection Using Threshold Value Classification Based on Thermographic Inspection. *Applied Sciences*, *11*(17), 7870.
[11] Takashimizu, Y., & Iiyoshi, M. (2016). New parameter of roundness R: circularity corrected by aspect ratio. Progress in Earth and Planetary Science, 3(1), 1-16.